Soft Matter

PAPER

View Article Online
View Journal | View Issue

Cite this: *Soft Matter*, 2022, **18**, 4378

Cell adhesion strength and tractions are mechano-diagnostic features of cellular invasiveness

Neha Paddillaya,[a] Kalyani Ingale,[b] Chaitanya Gaikwad,[c] Deepak Kumar Saini,[ad] Pramod Pullarkat,[e] Paturu Kondaiah,[d] Gautam I. Menon[fg] and Namrata Gundiah *[ac]

The adhesion of cells to substrates occurs *via* integrin clustering and binding to the actin cytoskeleton. Oncogenes modify anchorage-dependent mechanisms in cells during cancer progression. Fluid shear devices provide a label-free way to characterize cell–substrate interactions and heterogeneities in cell populations. We quantified the critical adhesion strengths of MCF-7, MDAMB-231, A549, HPL1D, HeLa, and NIH3T3 cells using a custom fluid shear device. The detachment response was sigmoidal for each cell type. A549 and MDAMB-231 cells had significantly lower critical adhesion strengths (τ_{50}) than their non-invasive counterparts, HPL1D and MCF-7. Detachment dynamics inversely correlated with cell invasion potentials. A theoretical model, based on τ_{50} values and the distribution of cell areas on substrates, provided good fits to results from de-adhesion experiments. Quantification of cell tractions, using the Reg-FTTC method on 10 kPa polyacrylamide gels, showed highest values for invasive, MDAMB-231 and A549, cells compared to non-invasive cells. Immunofluorescence studies show differences in vinculin distributions; non-invasive cells have distinct vinculin puncta, whereas invasive cells have more dispersed distributions. The cytoskeleton in non-invasive cells was devoid of well-developed stress fibers, and had thicker cortical actin bundles in the boundary. Fluorescence intensity of actin was significantly lower in invasive cells as compared to non invasive cells. These correlations in adhesion strengths and traction stresses with cell invasiveness may be useful in cancer diagnostics and other pathologies featuring mis-regulation in adhesion.

Received 4th January 2022,
Accepted 16th May 2022

DOI: 10.1039/d2sm00015f

rsc.li/soft-matter-journal

Introduction

Cell adhesions to substrates occur *via* integrin clustering. The binding of integrins to the actin cytoskeleton regulates essential cellular processes such as spreading, generation of contractility, migration, and cell cycle progression.[1,2] Oncogenes modify adhesion mechanisms during cancer progression, resulting in complex molecular cascades that alter the cell migration, proliferation, and invasion.[3–5] Changes to the cell–substrate adhesivity and E-cadherin abrogation are associated with the metastatic phenotype.[6,7] Cell stiffness correlates with metastatic and invasiveness potentials; transformed and metastatic cells demonstrate increased deformability as compared to non-invasive cells.[8,9] Focal adhesions, including integrins and other structural and signaling proteins, are altered and more dynamic in invasive cancer cells.[7,10,11] Integrin antagonists have been used in clinical trials to block cell proliferation, survival, and migration, as well as progression and metastasis.[12] The ability to measure the strength of cell adhesions to substrates and tractions is potentially helpful in targeted drug development for cancers. Such techniques also show promise in mechano-diagnostics, to sort cells with differential adhesion strengths, from a heterogeneous population of tumor cells.

Spinning disc devices use hydrodynamic shear stress, in the range of 0–100 Pa on cell-seeded substrates, to quantify the strength of adherent cells.[5,13,14] Because shear stresses vary along the radial direction in such studies, cells are subjected to differing stresses based on their location on the substrate.

[a] *Centre for Biosystems Science and Engineering, Indian Institute of Science, Bangalore, India*
[b] *Biological Sciences, Indian Institute of Science, Bangalore, India. E-mail: namrata@iisc.ac.in, ngundiah@gmail.com*
[c] *Department of Mechanical Engineering, Indian Institute of Science, Bangalore, India*
[d] *Department of Molecular Reproduction, Development and Genetics, Indian Institute of Science, Bangalore, India*
[e] *Soft Condensed Matter Group, Raman Research Institute, Bangalore, India*
[f] *The Institute of Mathematical Sciences, Chennai, India*
[g] *Departments of Physics and Biology, Ashoka University, Sonepat, India*

Experiments using spinning devices show exponential variation in the adhesive strengths with bond clusters.[13,14] More recent studies demonstrate heterogeneities in the adhesivity of cancer cells; strongly adherent cells were less migratory than metastatic cells.[15] Microscope mounted cone plate devices, with small cone angles, exert uniform fluid shear stress on cells.[16,17] Such devices also present advantages in permitting real-time visualization of the stress fibers and focal adhesions under physiologically relevant and controlled shear stress conditions (0–10 Pa). Earlier studies using such a device showed that the number of cells on the substrate decreased sigmoidally with increase in shear stress.[17] A theoretical model, incorporating stochasticity of cell adhesions to the substrate and population-level differences in cell sizes, was able to recapitulate the experimentally obtained detachment curves.[17] These studies suggested the importance of the adhesive areas in the critical shear stress required to detach cells from substrates. Other studies delineated weakly adhered cells from those with strong adhesions, in the presence of Mg^{+2} and Ca^{+2} ions, using parallel plate flow chambers.[18] Highly metastatic cells had weak adhesions and were characterized by the disassembling of focal adhesions.[19] Traction studies demonstrate that metastatic cells are significantly more contractile and have dynamic focal adhesions as compared to non-metastatic cells that have stronger adhesions.[19,20] Focal adhesions and stress fiber contractility are both important parameters in determining cell adhesions to substrates.[20]

We use a custom fluid shear device to obtain de-adhesion curves for cancer cells with differential invasiveness, including breast epithelial cells (MCF-7 and MDAMB-231), lung epithelial cells (A549 and HPL1D), HeLa, and NIH3T3 fibroblasts. We fit experimentally obtained de-adhesion data, and cell area distributions to the theoretical model developed by Maan and coworkers.[17] Results show that invasive cells, quantified using a transwell assay, have significantly lower detachment strengths as compared to the less invasive cells in our study. Cell adhesive areas increased with invasion potentials. The theoretical model was able to capture the sigmoidal detachment curves for all cell types in the study. Invasive cells also had higher tractions, obtained using a regularized FTTC approach, as compared to other cells.[21] A quantification of the cell–substrate adhesion strength is important in diseases, such as cancer, featuring mis-regulation in adhesion. The de-adhesion method may also be useful to separate heterogeneous populations of cells based on their adhesion potentials.

Methods

Cell culture

MCF-7, MDAMB-231, HPL1D,[22] A549, HeLa, and NIH3T3 cells in early passage were maintained in Dulbecco's Modified Eagle Medium (DMEM, Invitrogen) supplemented with 10% (v/v) fetal bovine serum (FBS, Invitrogen) and 1% (v/v) penicillin/streptomycin (Sigma-Aldrich) in a humidified incubator containing 5% CO_2 at 37 °C. Cells were passaged every 2–3 days during the study.

Transwell invasion assay

Trans-well chambers (24 well, 8 μm pore-size, Corning) were used to quantify the cell invasion potentials. Collagen I (Gibco; 1 mg ml^{-1}) was incubated on the membranes overnight. A suspension of serum-starved cells (5×10^4 in 200 μl of DMEM without FBS) was seeded on each insert within the well. Uncoated inserts were used as controls. The invasion chambers were incubated overnight with 800 μl of DMEM with 10% FBS to permit cell migration, the inserts were fixed and washed twice with PBS, and the cells removed using a cotton swab. Crystal violet staining solution (0.5%) was added to each insert for 10 minutes which was followed by acetic acid solution (33%). The insert was placed on a rocker for 10 minutes, and the eluent from the well was transferred to a 96-well clear microplate (Thermo). The absorbance was measured at 590 nm using a plate reader. Cell invasion fraction was calculated as:

$$\text{Invasion} = \frac{\text{Absorbance of Control inserts}}{\text{Absorbance of Collagen-I coated inserts}} \quad (1)$$

Measurement of the cell areas and immunofluorescence analysis

Cells were cultured on 22 mm coverslips, rinsed twice with chilled phosphate-buffered saline (PBS, Sigma Aldrich, D5652), and fixed with 4% paraformaldehyde solution for 15 minutes. To quantify the adhesive areas, cells were stained using rhodamine–phalloidin (1 : 200, Invitrogen, R415) at room temperature in an antibody staining buffer. These data were used to obtain the cell areas ($N \sim 100$) for each group using Fiji (ImageJ). Data from adhesive areas in each cell group were fit to a log-normal distribution to obtain the mean, μ, and standard deviation of the logarithmic values, s.

Specimens were permeabilized with 4% paraformaldehyde and incubated for 1 hour at room temperature in primary antivinculin (1 : 500, Sigma Aldrich, V4505), secondary antibody, Alexa Fluor 488 (1 : 600, Invitrogen, A32723), and rhodamine–phalloidin (1 : 200, Invitrogen, R415) at room temperature in staining buffer to visualize stress fibers and vinculin. Cell nuclei were labelled with DAPI (1 : 500, Thermo, 62248) for 2 minutes, and the samples were rinsed thrice with PBS. Specimens were fixed with ProLong™ Diamond Antifade Mountant (Invitrogen, P36961), and imaged using a confocal microscope (Leica SP8, Bioimaging facility, IISc, Bangalore). Fiji by ImageJ was used to calculate the fluorescence intensities of vinculin and actin in each cell. The intensity values were corrected for background noise, and total intensity per unit cell area was obtained for each of the different cell groups in the study (n = 29 to 36 for each group).

Fluid shear experiments using the microscope mounted device

Glass coverslips (22 mm, Bluestar) were cleaned, air-dried, and attached to a 60 mm cored Petri plate using a thin layer of vacuum grease. Coverslips were plasma-activated for 2 minutes and coated with 40 μg ml^{-1} collagen I (Gibco) at 37 °C for

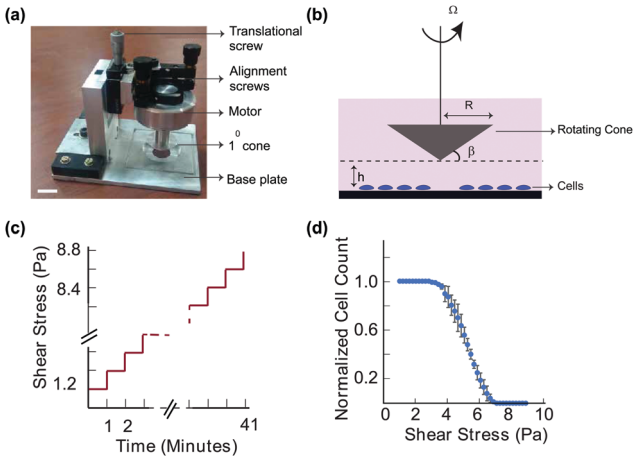

Fig. 1 (a): The image shows a custom-fabricated, microscope mountable, fluid shear device used in the study. Device parts are labelled and include a 1° cone which is rotated using a motor on a Petri dish containing adherent cells. The motor is aligned to ensure that the cone is orthogonal to the base plate. A translational stage helps position the cone at a predetermined height relative to the base plate. Scale bar = 10 mm. (b) Couette flows are generated through rotation of the cone using a controlled program to exert shear stresses on the cells. (c) Shear stresses were increased in steps of 0.2 Pa at each minute, and images of the cells were taken using an inverted microscope. (d) Results are plotted showing the normalized cell number on the plate is shown with shear stress for a representative HeLa sample.

1 hour in a humid chamber. Substrates were washed three times with phosphate-buffered saline (PBS), and cells were seeded at 5000 cells per ml for 12 hours to permit attachment and spreading. Low cell seeding densities were used to minimize the contributions from cell–cell interactions in the analyses. Cell cycles were not synchronized and included those in the G2/M phase. Hoechst (1 : 400; Thermo Scientific) was used to stain the nuclei for 3 minutes before the de-adhesion experiments. The cell-seeded Petri dish was placed on the base plate of the fluid shear device on an inverted microscope (Leica DMI6000B with PeCon incubator) maintained at 5% CO_2 at 37 °C (Fig. 1a). The device works broadly on the principle of a cone-plate rheometer, and uses Couette flows to subject cells to shear stress (Fig. 1b).[17] A conical disc with 1° cone angle (β) was attached to a motor, extracted from a computer hard drive, and driven using an Electronic Speed Controller (ESC). The device was powered using a DC power supply, and an Arduino UNO circuit was used to control the pulse width modulation signal.[23] The cone was rotated at different speeds using a custom program, and the speed of rotation, ω, was determined using a tachometer. Levelling screws on the device were used to align the cone parallel to the Petri dish. The cone was positioned ~10 μm above the base plate using a translation stage, and the fluid shear stress was increased in 0.2 Pa steps each minute using the ESC (Fig. 1c). Shear stress, τ, was calculated using the fluid viscosity, μ, cone angle, β, and rotation, ω, as

$$\tau = \frac{(\omega \times \mu)}{\beta} \quad (2)$$

Images of cells, acquired during each increase of shear stress, were analyzed using Fiji (ImageJ) to obtain the number of cells remaining on the substrate. The normalized cell number was plotted with increasing shear stress to obtain the detachment response of cells (Fig. 1d). Experiments were performed in biological triplicates, consisting of ~100 cells for every run, for each of the six cell types in the study. Data are reported as Mean ± SD. Detachment stresses were compared between the various cell groups using a one-way analysis of variance (ANOVA) with Bonferroni comparisons to test for individual differences between the groups. Statistical differences ($p < 0.05$) are indicated.

Theoretical model for de-adhesion of attached cells under fluid shear

Experimentally obtained data were used in the theoretical model developed for cell detachments under fluid shear by Maan and co-workers.[17] The cell was approximated to be a solid hemisphere, and was assumed to have a uniform distribution of focal adhesions along the perimeter. The model cell was subjected to Stokes flow, characterized by low Reynolds numbers, and the kinetics of adhesions to the substrate were described using the Bell's model. Based on this model, the attachments between a cell and the substrate form at a rate, k_{on}, and break exponentially with the applied stress.[24] The number of cells remaining on the substrate, $\Phi(t)$, under a controlled increase in the fluid shear stress, t, is given by

$$\Phi(\tau) = \frac{1}{2}\left[1 - erf\left(\frac{\ln\left(\frac{\tau}{\tau_{50}}\right)}{\sqrt{2}s}\right)\right] \quad (3)$$

τ_{50} is the critical shear stress corresponding to 50% cells remaining on the substrate with increase in fluid shear. The parameter, s, in eqn (3) was estimated using the best fit to cell area distributions as described earlier. This value is hence proportional to the areal width of the distributions.

To compare model predictions with experimental data, we used the poly-area function in MATLAB (v R2019b, The MathWorks Inc. Natick, MA). This function computes differences in the areas between two curves. Smaller values of poly-area indicate better fits of the model predictions with experimental data as compared to larger poly-area values.

Traction force microscopy

Cleaned coverslips were treated at room temperature with 3-amino-propyl triethoxy silane (Sigma Aldrich) and incubated with 0.5% glutaraldehyde solution (SDFC Ltd) for 30 minutes. Another set of cleaned coverslips was treated with poly-L-lysine (Sigma Aldrich) for 45 minutes at 37 °C in a humid chamber. A 18 μl ml^{-1} of 2% stock fluorescent beads (Invitrogen, F8810) was spin-coated on the coverslip using a previously published protocol.[21] Solutions of acrylamide (PA; 40% wt/vol, Sigma Aldrich) and *N*,*N*′-methylene bis-acrylamide (2% wt/vol, Sigma Aldrich) were mixed with distilled water.[25] 30 μl of the solution was combined with 10% APS (Thermo, 17874) and TEMED (Thermo, 17919), sandwiched between the cleaned and bead coated coverslips, and polymerized at room temperature for

30 minutes to obtain gels of 10 kPa stiffness. The bead-coated coverslip was carefully removed from the polyacrylamide gel and attached to a 35 mm punched Petri dish (Nunc, Thermo Scientific) using a thin layer of vacuum grease (SDFC Ltd). A solution of heterobifunctional sulpho-SANPAH linker (200 μl of 100 mg ml^{-1} stock; Thermo, A35395), diluted in HEPES buffer (50 mM; Sigma Aldrich, H3375), was pipetted to the gel surface. The assembly was exposed to 365 nm UV light (Thermo, 95034) for 10 minutes. Collagen-I (100 μl of 80 μg ml^{-1} concentration) was incubated on the gel surface at 37 °C for 45 minutes in a humid chamber.

Substrates were rinsed thrice with HEPES buffer, and 200 ml of cells (2000 cells per ml) was seeded on the gels for 12 hours. The experiment was performed in a live cell chamber at 37 °C and 5% CO_2 (Leica DMI6000B with PeCon incubator; 40× oil immersion objective). Three images were used for each attached cell; first, a phase-contrast image to obtain the cell boundary. Second, a fluorescent image of beads on the gel surface with the attached cell (stressed configuration), and finally, an image of the beads (referential configuration) following trypsinization (Sigma Aldrich). These images were used to quantify the constrained traction stresses exerted by cells on the substrate using a regularized Fourier Transform Traction Cytometry (Reg-FTTC) method in MATLAB.[21] Experiments were performed in triplicates for each of the different cell types in the study. Results from n = 10 are reported for each cell group in the study.

Results and discussion

Higher cell invasiveness correlates with lower cell adhesion strengths

To obtain the de-adhesion strengths, fluid shear stress was ramped as described earlier, and the number of cells remaining on the substrate was measured for each of the six different cell types in the study (Fig. 1a). These include an embryonic mouse fibroblast (NIH3T3), human cancer cells of varying invasion potentials, and non-invasive cells. The HPL1D is an immortalized non-invasive lung epithelial cell, whereas A549 cells are invasive lung adenocarcinoma cells. MCF-7 is a non-invasive breast cancer cell as compared to the invasive MDAMB-231 cells. We also used HeLa cells which are metastatic cervical cancer cells in the study.

The cell detachment responses were sigmoidal for all cell types; shapes and shifts of the detachment curves were however significantly different for all groups in the study. We delineated the detachment responses based on three different magnitudes of shear values (Fig. 2a). τ_{10} is the threshold shear stress, required to detach 10% of cells from the substrate, which helps identify loosely or weakly adhered cells on the substrate. τ_{50} is the characteristic critical de-adhesion strength based on the detachment of 50% cells from the substrate under shear. Finally, τ_{90} shows the percentage of cells remaining on the substrate under fluid shear which have strongly adherent cells and those that may remodel in response to increasing shear

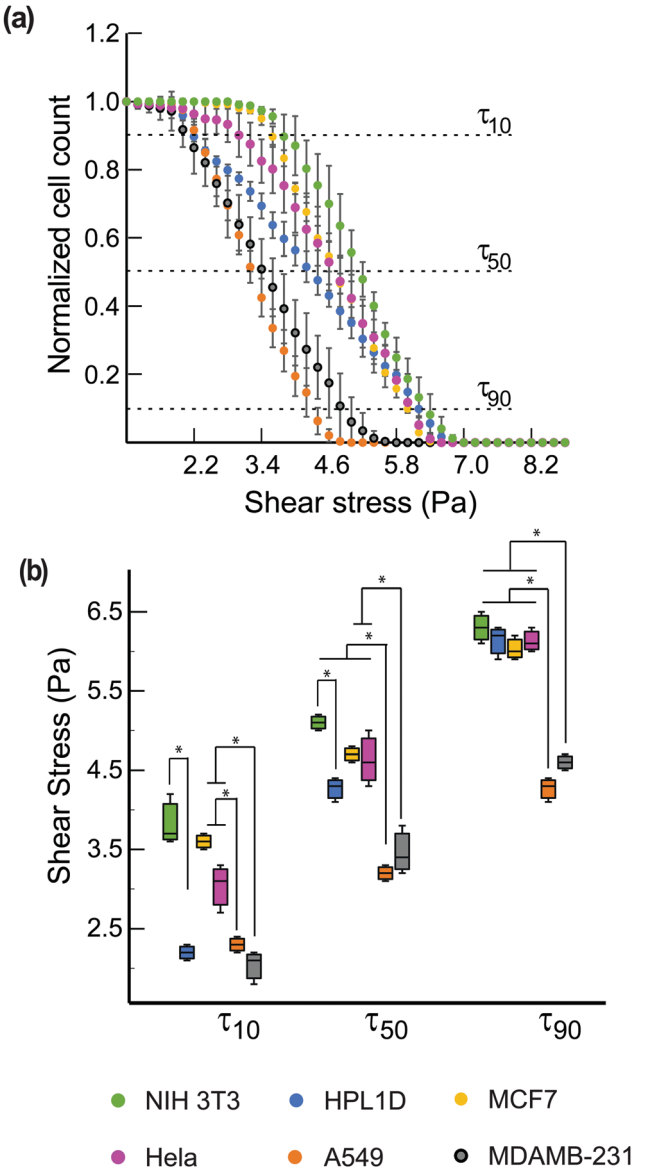

Fig. 2 (a): Normalized cell count, calculated as the number of cells at a given time relative to the initial cell number, is plotted as a function of shear stress for each of the six different cell types in the study. Data are represented as Mean ± SD. (b) The de-adhesion strengths corresponding to τ_{10}, τ_{50}, and τ_{90} were compared between the different groups. Statistically significant differences ($p < 0.05$) are indicated by (*).

stress. We compared the detachment strengths, obtained from experiments at τ_{10}, τ_{50} and τ_{90}, with the invasive potentials of cells in the study.

More invasive cells, A549 and MDAMB-231, had significantly lower critical detachment strengths, τ_{50}, as compared to the non-invasive MCF-7 (Fig. 2b; Table 1). HeLa cells had significantly higher τ_{50} values than the MDAMB-231 and A549 cells (Fig. 2b and Table 1). Normal lung epithelial cells (HPL1D) had significantly higher τ_{50} values as compared to the more invasive (A549) cells. NIH3T3 cells had the highest critical detachment strength in the study (Table 1). Critical detachment strength hence shows an inverse correlation with the invasive potential

Table 1 Critical deadhesion strengths (τ_{50}) obtained from the experiments, and cell area parameters (n = 100 in each group) from the log-normal distribution (μ, s) were used in the theoretical model to quantify cell detachment from the substrate under fluid shear

	τ_{50} (Pa) (Mean ± SD)	Cell area (μm^2)	μ	s	χ^2
NIH3T3	5.1 ± 0.10	1928.06 ± 481.79	7.54	0.25	3.73
HPL1D	4.27 ± 0.15	1866.76 ± 452.11	7.50	0.24	2.24
MCF-7	4.70 ± 0.10	757.71 ± 151.22	6.61	0.21	1.65
HeLa	4.63 ± 0.35	880.95 ± 162.44	6.76	0.19	1.32
A549	3.20 ± 0.10	1049.68 ± 170.65	6.94	0.16	2.93
MDAMB-231	3.47 ± 0.31	1248.01 ± 254.25	7.11	0.20	6.16

of cells. The threshold de-adhesion values of shear (τ_{10}) were also clearly different in the various cell types in our study. Fibroblasts (NIH3T3) had the highest values of τ_{10} (3.83 ± 0.32 Pa), whereas the metastatic cells (A549 and MDAMB-231) had significantly weaker adhesions characterized by low values of τ_{10}. The non-invasive MCF-7 cells had significantly higher values of τ_{10} as compared to the more invasive cells in the study. HPL1D cells had lower τ_{10}, and very high values of τ_{90}, which suggests heterogeneity in the cell adhesion strengths. These cells were maintained in DMEM with serum and antibiotics. Earlier studies on HPL1D cells used media that included several additional growth factors.[22] Although the cell morphologies were not different in this population in our study, the de-adhesion experiments show clear differences in the adhesiveness which may be attributed to the differing cell culture conditions. Cancer cells with higher invasive potentials, A549 and MDAMB-231, had significantly lower values of τ_{90} under sustained shear as compared to other cells. There were no differences in these values for all other cell groups.

A log-normal distribution provided good fits to the experimentally measured spread areas for all cell types in the study (Fig. 3 and Table 1). MCF-7, HeLa, and A549 cells had a narrow distribution of areas as compared to other cells in the study. NIH3T3 and HPL1D cells had higher mean spread areas and larger standard deviations. Results from the invasion assay (Fig. 4a) demonstrate the highest invasion potential for

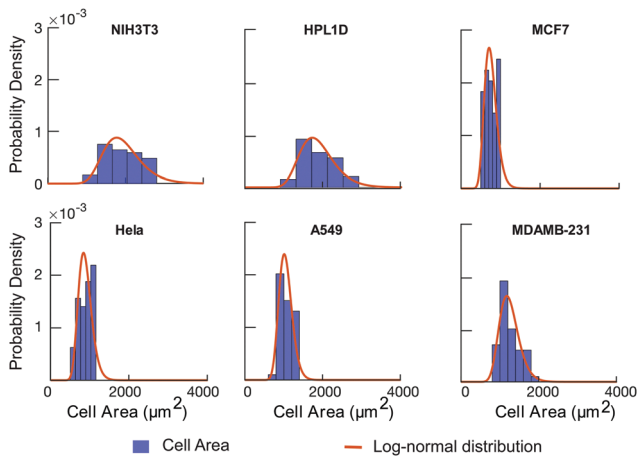

Fig. 3 Cell spread areas (Mean ± SD) for each group (n = 100) were plotted and the data were fit to a log-normal distribution function.

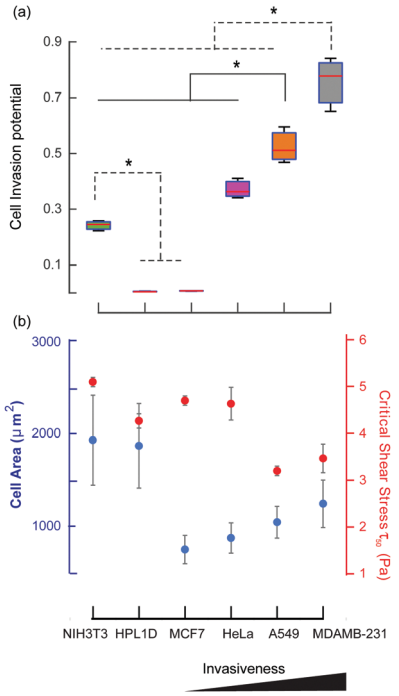

Fig. 4 (a) Results from the invasion assay show ratio of invaded cells relative to control inserts for each of the different cell types in the study. Differences between the groups are indicated in the figure (* $p < 0.05$). (b) Cell areas and critical shear stresses (τ_{50}) were plotted based on the cell invasiveness.

MDAMB-231 cells (0.76 ± 0.10), followed by A549 cells (0.53 ± 0.06) and HeLa cells (0.37 ± 0.04). NIH3T3 cells had a relatively low ratio (0.24 ± 0.02) of invasion. In contrast, the MCF-7 (0.01 ± 0.00) and HPL1D (0.01 ± 0.00) cells had the lowest values of invasion. We plotted the mean cell areas and critical detachment strengths (τ_{50}) to investigate possible correlations between these parameters (Fig. 4b). Cell areas showed a linear increase with higher cell invasiveness potentials. Although the MCF-7 and A549 cells had similar projected areas, the former had a significantly higher value of critical detachment strength (τ_{50}) as compared to A549 cells. Comparisons between the MCF-7 and MDAMB-231, and the HPL1D and A549 groups show that more invasive cells within the groups required lower critical shear stress to detach as compared to those with lower invasive potentials.

HPL1D cells required higher critical shear stress to detach and had greater cell spread areas as compared to all other cancer epithelial cells in the group. NIH3T3 fibroblasts had the highest critical stress to detach from substrates (5.1 ± 0.10 Pa), and the highest mean area in the study. These data suggest that a small population of strongly adherent cells, remaining under sustained shear, may be due to cell polarizations and remodeling. The sigmoidal detachment profiles obtained in this study are similar to the results reported by Maan *et al.* for HEK and NIH3T3 cells using a similar device.[17]

Other studies have also reported de-adhesion profiles with marginally different critical detachment strengths for various cell types, including osteosarcoma cells, NIH3T3,

WI38 fibroblast, Swiss 3T3 murine fibroblast, among others.[13,18,26–28] Cancer cells regulate cell–substrate interactions during the various stages of metastasis through changes in their adhesion kinetics.[29] The types of integrins in breast cancer cells (αvβ5/αvβ3 and α5β1/α2β1) also change under static and shear flow conditions.[30] Variations in the adhesion strengths of cancer cells may also depend on the cell type, differences in the integrin types, and the presence of oncogenes, such as ERBB2 induced during metastasis.[31–33] Less metastatic (HT-29P) cells had six times higher adhesion strengths than the highly metastatic HT-29LMM on collagen-1 substrates; these adhesions were however not different on fibronectin-coated substrates.[34] Marginal differences in the critical detachment strengths of cells in our study to those reported earlier may be due to the differences in the extracellular matrix type, ligand densities, and the application of shear stress using media in this study as compared to the use of PBS.[16,18,28] Cell detachment studies hence provide a quantitative measure of the differences in adhesion kinetics between cells of varied invasive potentials.

Modelling cell detachments from substrates using τ_{50} and cell adhesive areas

We used the experimentally measured critical de-adhesion strengths (τ_{50}) and adhesive areas of cells on ligand coated substrates (Fig. 3) to test model predictions for the various cell types in our study (Fig. 5). Because experimentally obtained cell de-adhesion results were not symmetric relative to the critical shear stress value (τ_{50}), we used the function poly-area to compare results below τ_{50} and those greater than τ_{50} with experimental data (Table 2). The model fit experimental data for the MCF-7 cells below (poly-area: 1.16) and above τ_{50} (poly-area: 2.25). We see similar results for the HeLa and A549 cells (Table 2).

NIH3T3 and MDAMB-231 cells, which have elongated morphologies, deviated significantly from the spherical cell shape assumed in the model; the poly-area values are hence high for both these cell types. Results from fits to the HPL1D cells showed maximum differences with experiments. The shear de-adhesion experiments may hence be useful to delineate possible heterogeneities in cell populations. Deviations from the model may also be related to possible cell remodeling and reinforcements in the adhesions under sustained shear.[35] In contrast, τ_{10} values were overpredicted by the model, as compared to experimentally obtained values for MDAMB-231 and HPL1D cells. These differences may either be due to weak adhesions or possible biological heterogeneities within the cell populations which were not assessed in this study.

Table 2 Poly-area function were was used to compare deviations of the model predictions with the experimental data at regions below τ_{50} and those above this value. Low values of poly-area suggest good fits of the model to experiments

Poly-area	Below τ_{50}	Above τ_{50}
NIH3T3	1.46	4.23
HPL1D	5.13	3.54
MCF-7	1.16	2.25
HeLa	2.34	1.25
A549	2.15	2.37
MDAMB-231	3.22	2.26

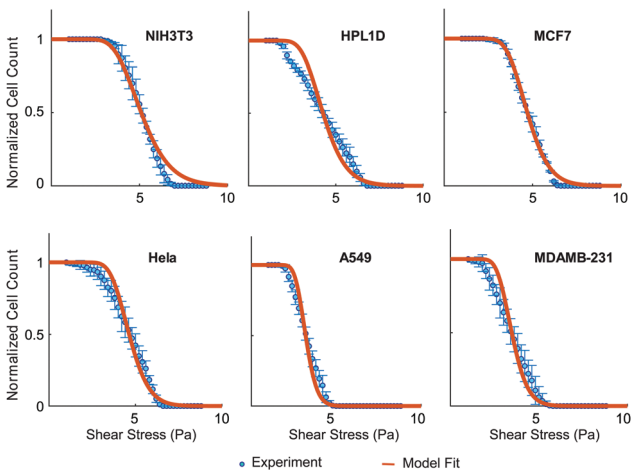

Fig. 5 Model predictions show good fits with experimental data for all cell types. The model uses τ_{50} values, and the mean, μ, and SD, s, values from the areal distributions for each cell type in the study.

Cells form integrin-mediated adhesions with the substrate at the leading edge, and disintegrate at the retracting end during migrations. Adhesions strengthen during cell spreading and result in an increase in the cell–substrate contact area, receptor clustering, and focal adhesion assembly, through interactions with the cytoskeleton[36] and the bound integrins.[5] A higher ECM ligand density also controls cell spreading through focal adhesion assembly. Cell spreading regulates function through changes in the morphology and cytoskeletal tension.[37,38] Modifications to the model, including variations in the cell shape under shear, possible redistributions in focal adhesions due to cell polarizations, and varying stress fiber contractility, may be useful in future studies to better estimate the marginal deviations in the detachment profiles of cells from substrates. The theoretical model, based on τ_{50} and the adhesive areas of contact between the cell and the substrate, is however useful to delineate the differences in critical de-adhesion strengths between cell types.

Invasive cells exert higher traction stresses

We used traction force microscopy to quantify the differences in cell contractility in the different cell types (Table 3) using 10 kPa polyacrylamide gels ($n = 10$ in each group). Fig. 6a shows the maximum tractions exerted by adherent cells on substrates obtained using the Reg-FTTC approach.[21] There were no statistical differences in maximum tractions between MCF-7 (294.45 ± 48.74 Pa) and HeLa cells (293.58 ± 36.32 Pa) that had the lowest tractions among all cells in the study (Table 3). In contrast, the MDAMB-231 cells had the highest tractions (2050.82 ± 127.29 Pa), followed by the A549 invasive cancer cells (1116.24 ± 86.71 Pa). NIH3T3 fibroblasts and normal lung epithelial cells (HPL1D) had intermediate tractions (833.12 ±

Table 3 Results from traction force cytometry (FTTC) are shown for all cells in the study (Mean ± SD). Values obtained from constrained and regularized approaches (Reg-FTTC) are presented, and the range of regularization parameters are indicated (n-10 each cell type)

	Max traction (FTTC) (Pa)	Max traction (Reg-FTTC) (Pa)	Regularization parameter (γ^*) range
NIH3T3	1032.14 ± 290.95	833.12 ± 215.01	2.053 to 2.244 × 10^{-11}
HPL1D	1017.29 ± 590.73	820.58 ± 483.65	2.054 to 2.539 × 10^{-11}
MCF-7	358.22 ± 114.87	293.58 ± 102.84	4.071 to 5.411 × 10^{-11}
HeLa	372.76 ± 154.13	294.45 ± 125.38	1.572 to 1.573 × 10^{-10}
A549	1398.07 ± 274.19	1116.24 ± 228.94	4.067 to 1.13 × 10^{-10}
MDAMB-231	2628.62 ± 402.53	2050.82 ± 308.33	1.443 to 5.411 × 10^{-11}

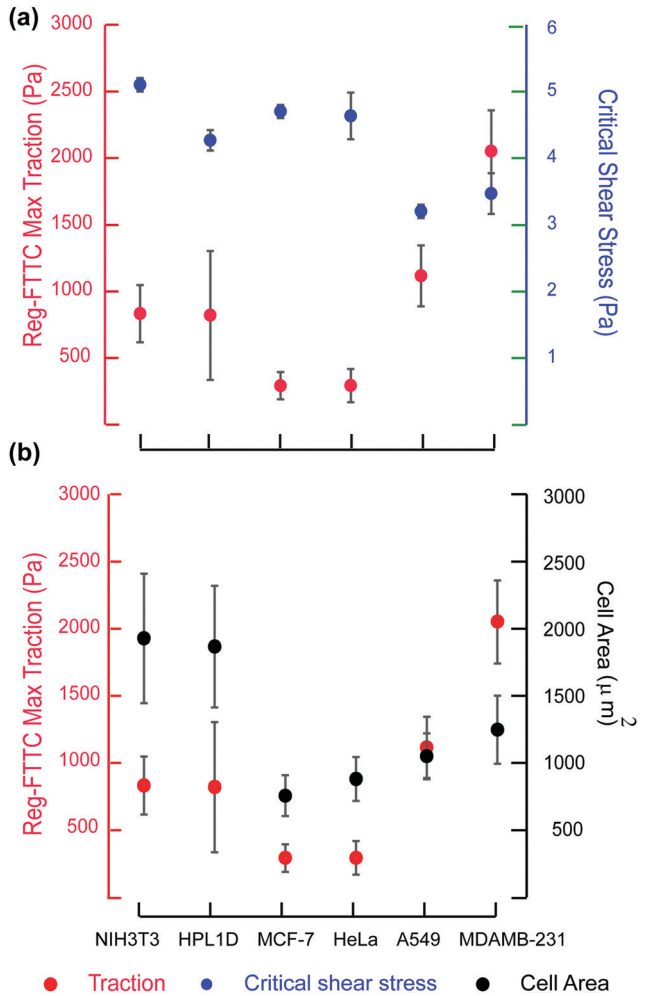

Fig. 6 Reg-FTTC tractions were calculated and plotted as Mean ± SD in the study (n = 10 in each group). (a) Cells with lower critical shear stress show higher tractions. (b) Cell areas and tractions increased with invasiveness potential.

92.01 Pa and 820.58 ± 186.81 Pa, respectively), which were higher than the non-metastatic cells, and lower than corresponding metastatic cells. Bead density and distribution, and the presence of small filopodial protrusions contribute to errors in the calculation of cell tractions.[39] We have hence compared the maximum tractions between the different cell types in this study.

The Reg-FTTC approach uses a regularization parameter (γ^*), which is determined using an inflection point in the plots of the maximum tractions with the log of the regularization parameter.[21] Although the maximum tractions obtained using Reg-FTTC were lower than those obtained using the FTTC approach, similar trends were visible for the different cell types in this study. Invasive (A549 and MDAMB-231) cells had the lowest critical de-adhesion strengths and higher tractions as compared to all other cells in the study (Fig. 6a). NIH3T3 cells had higher de-adhesion strengths and tractions as compared to non-invasive cells (MCF-7 and HeLa). Our results hence suggest the importance of cell contractility during adhesions to substrates.

The spread areas for the different cell types were next plotted to explore possible correlations with tractions (Fig. 6b). Cells with greater invasiveness potentials exerted higher traction stresses on 10 kPa gels as compared to cells with lower invasion potentials in our study. These data agree with earlier studies which show that metastatic cells exert higher traction stress as compared to non-metastatic cells.[20] Tumor-associated endothelial cells also exert higher tractions than normal endothelial cells.[40] In contrast, murine breast cancer cells with higher metastatic potential, and Ras-transformed fibroblasts, showed weak traction stresses.[10,41] H-ras transformed 3T3 fibroblasts exert lower tractions than normal 3T3 fibroblasts cells.[42] Lung and breast cancer cells with higher invasion potentials generate higher 3D tractions as compared to their counterparts with lower invasive potentials.[43] Sen and Kumar showed a sigmoidal decrease in the cell adhesive area with time, following trypsin treatment, which suggest the importance of actomyosin contractility in cell adhesions to substrates.[44] Focal adhesions and stress fibers are hence essential in traction generation by adherent cells on substrates. The traction stresses exerted on substrates may hence be used as a biophysical marker of the metastatic potential and malignancy of cells.[20,43,45]

The cytoskeleton and invasiveness potential of cells

Faster cell detachment in cell types with higher invasion potential suggests a possible role for cell contractility and focal adhesions. We stained for actin and vinculin distributions to visualize differences among the different cell types in the study. Immunofluorescence studies show differences in vinculin distribution in the various cell lines (Fig. 7). Cells with lower invasion potentials had distinct and well-formed vinculin puncta that are reminiscent of stationary and less migratory cells. The cytoskeleton in these cells also has thick cortical actin bundles and lacks well-developed stress fibers (Fig. 8). In contrast, cells with higher invasion potential had diffuse

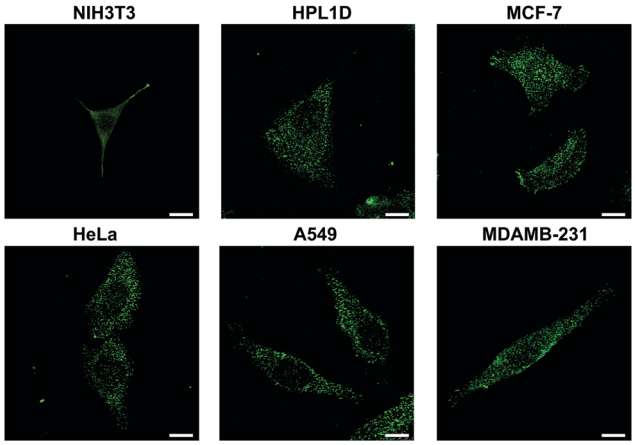

Fig. 7 Focal adhesion sizes and distribution are visibly different for cells with differential invasiveness potentials. Vinculin in the focal adhesions is labelled in green. Scale bar = 10 μm.

vinculin. Lamellipodia and protrusions are clearly visible in the migratory cancer cells. We used confocal microscopy images to quantify the vinculin and actin fluorescence intensities for each cell in teh six different groups in our study. Fluorescence intensities per unit cell were highest for the HPL1D, MCF-7 and HeLa cells. Highly contractile NIH3T3 cells and invasive cells (MDAMB-231 and A549) had lower actin intensity per unit cell (Fig. 9a).

Highly migratory cells (MDAMB-231 and NIH3T3) showed the highest vinculin intensity per unit cell due to the presence of more dynamic focal adhesions throughout the cell (Fig. 9b).

The differences in focal adhesion assembly, migration, and contractility determine the invasion potentials which is linked to the downregulation of E-cadherin in cells that undergo the epithelial-to-mesenchymal transitions (EMT).[46] Genetic and environmental cues cause changes to the adhesions during EMT which result in heterogeneities in the adhesive phenotype.[47,48] Beri *et al.* delineated weakly and strongly

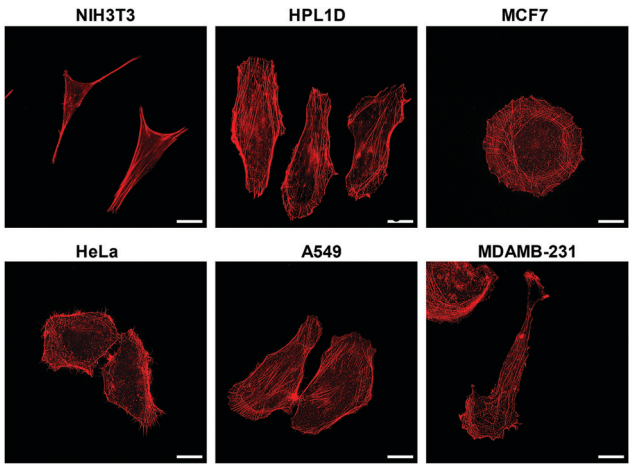

Fig. 8 F-actin-stained images show prominent stress fibers in invasive cells. Non-invasive cells showed actin at the boundary and cortex. Actin is labelled in red. Scale bar = 10 μm.

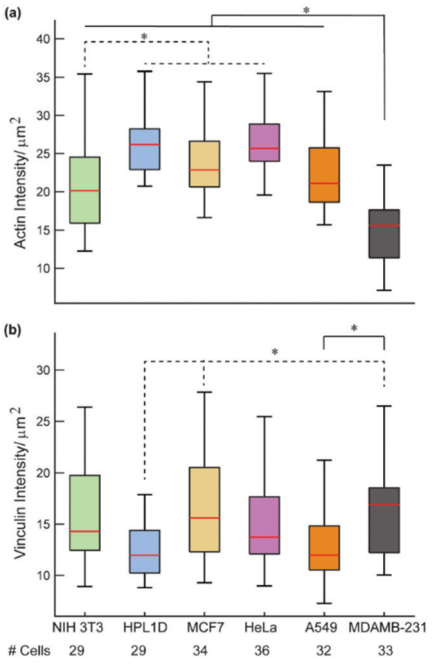

Fig. 9 Fluorescence intensities were quantified per unit cell area for (a) actin and (b) vinculin. Significant differences between groups are indicated (*$p < 0.05$).

adherent cells using fluid shear from cell populations.[19] Heterogeneity in cancer cells may be genetic, epigenetic, transcriptomic, proteomic, and functional.[49] Cancer cells actively modify their spreading,[50,51] and migration[52,53] behaviors in response to biophysical cues. Clonal heterogeneity analysis is useful to predict the patient prognosis and response to therapy. Fluid shear stress experiments may be useful in delineating heterogeneities in cell populations based on the cell adhesion strengths to substrates.

Conclusions

Cancer metastasis is characterized by the local invasion of cells from primary tumors, their transport through systemic circulation, their extravasation to secondary sites, and the growth of metastatic lesions in those sites.[54] The invasive ability of cancer cells through the three-dimensional tissue milieu correlates with their ability to modulate their adhesion strengths which we have quantified using fluid shear on a planar substrate plated with cells. Experiments using a fluid shear device are useful to delineate differences in adhesion strengths between cancer cells, sort cells based on differential adhesion abilities, and quantify the differences in the roles of adhesions during cancer metastasis. We provide a quantitative measure of the adhesive state of a cell. We hope that such methods, combined with an understanding of the molecular mechanisms, will help better understand cancer metastasis.

Results from our experiments show that cell areas, tractions and critical adhesion strengths are determininstic factors in cellular adhesions to substrates (Fig. 10). Lower adhesion

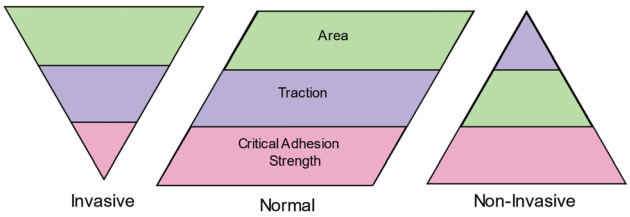

Fig. 10 The relative roles of cell areas, tractions and critical adhesion strengths are shown for the three different cell types in the study.

strengths for highly invasive, polarized and migratory cells correlated with high traction stresses and adhesive areas. These results suggest that drug treatments to alter cell contractility may be useful in cancer management. The adhesive heterogeneity within a tumour population may also be delineated based on the critical adhesion strength and cell tractions.

Migration is inhibited in cells that firmly adhere to the ECM.[55] We show that more metastatic cells have lower adhesion strength than non-metastatic cells, whereas normal cells have higher adhesion strength than cancer cells. The theoretical model of Maan *et al.* fits the de-adhesion profiles for all cell types in our study.[17] A marginal deviation from the predicted sigmoidal behaviour may arise due to differential contractility, assumptions regarding the FA size and distribution, and the differences in cell shapes that are not included in the model.

Focal adhesions are more prominent in non-invasive cells as compared to invasive and normal cells (Fig. 7). The adhesion strength and traction measurements are hence useful biophysical markers of cell metastasis. Inherent differences in the differential adhesion strengths may help sort cells with varying invasive potentials. Additional experiments with inhibitors for proteins involved in cell–substrate mechanics and contractility will be useful in understanding the functional regulatory circuits that may be involved in these interactions and in the design of better therapeutic options.

Author contributions

NP performed all experiments, analyzed results, and helped write the manuscript. KI helped perform the traction experiments, and CG helped with the device design. DKS and PK provided inputs with cell culture and immunofluorescence studies. PP, GIM, and NG designed the study and analyzed the results. NG wrote the manuscript with inputs from all authors.

Conflicts of interest

All authors declare that they do not have any conflict of interest.

Acknowledgements

We thank the imaging facility in Biological Sciences, IISc, for the confocal imaging reported in this study. We thank the members of the mechanical workshop at Raman Research Institute for help with device fabrication. PK and DKS laboratories are supported by the IISc-DBT partnership program and DST-FIST infrastructure to MRDG. PK is a recipient of senior scientist fellowship from the Indian National Science Academy. PP, GIM, and NG are grateful to the Department of Biotechnology for project support through a jointly funded grant.

References

1 R. Zaidel-Bar, M. Cohen, L. Addadi and B. Geiger, Hierarchical assembly of cell-matrix adhesion complexes, *Biochem. Soc. Trans.*, 2004, **32**(3), 416–420, DOI: **10.1042/BST0320416**.
2 J. D. Humphries, A. Byron and M. J. Humphries, Integrin ligands at a glance, *J. Cell Sci.*, 2006, **119**(19), 3901–3903, DOI: **10.1242/jcs.03098**.
3 M. A. Schwartz, Integrins, oncogenes, and anchorage independence, *J. Cell Biol.*, 1997, **139**(3), 575–578, DOI: **10.1083/jcb.139.3.575**.
4 N. Reymond, J. H. Im, R. Garg, F. M. Vega, B. B. D'agua, P. Riou, S. Cox, F. Valderrama, R. J. Muschel and A. J. Ridley, Cdc42 promotes transendothelial migration of cancer cells through β1 integrin, *J. Cell Biol.*, 2012, **199**(4), 653–668, DOI: **10.1083/jcb.201205169**.
5 N. D. Gallant, K. E. Michael and A. J. García, Cell adhesion strengthening: Contributions of adhesive area, integrin binding, and focal adhesion assembly, *Mol. Biol. Cell*, 2005, **16**(9), 4329–4340, DOI: **10.1091/mbc.E05-02-0170**.
6 U. Cavallaro and G. Christofori, Cell adhesion and signalling by cadherins and Ig-CAMs in cancer, *Nat. Rev. Cancer*, 2004, **4**(2), 118–132, DOI: **10.1038/nrc1276**.
7 S. A. Brooks, H. J. Lomax-Browne, T. M. Carter, C. E. Kinch and D. M.-S. Hall, Molecular interactions in cancer cell metastasis, *Acta Histochem.*, 2010, **112**(1), 3–25, DOI: **10.1016/j.acthis.2008.11.022**.
8 E. M. Darling and D. Di Carlo, High-throughput assessment of cellular mechanical properties, *Annu. Rev. Biomed. Eng.*, 2015, **17**, 35–62, DOI: **10.1146/annurev-bioeng-071114-040545**.
9 A. H. Kulkarni, A. Chatterjee, P. Kondaiah and N. Gundiah, TGF-β induces changes in breast cancer cell deformability, *Phys. Biol.*, 2018, **15**(6), 065005, DOI: **10.1088/1478-3975/aac3ba**.
10 I. Indra, V. Undyala, C. Kandow, U. Thirumurthi, M. Dembo and K. A. Beningo, An in vitro correlation of mechanical forces and metastatic capacity, *Phys. Biol.*, 2011, **8**(1), 015015, DOI: **10.1088/1478-3975/8/1/015015**.
11 W. H. Guo and Y. L. Wang, Retrograde fluxes of focal adhesion proteins in response to cell migration and mechanical signals, *Mol. Biol. Cell*, 2007, **18**(11), 4519–4527, DOI: **10.1091/mbc.E07-06-0582**.
12 J. S. Desgrosellier and D. A. Cheresh, Integrins in cancer: Biological implications and therapeutic opportunities, *Nat. Rev. Cancer*, 2010, **10**(1), 9–22, DOI: **10.1038/nrc2748**.

13 A. J. García, P. Ducheyne and D. Boettiger, Quantification of cell adhesion using a spinning disc device and application to surface-reactive materials, *Biomaterials*, 1997, **18**(16), 1091–1098, DOI: 10.1016/S0142-9612(97)00042-2.
14 A. J. García, F. Huber and D. Boettiger, Force required to break α5β1 integrin-fibronectin bonds in intact adherent cells is sensitive to integrin activation state, *J. Biol. Chem.*, 1998, **273**(18), 10988–10993, DOI: 10.1074/jbc.273.18.10988.
15 A. Fuhrmann, A. Banisadr, P. Beri, T. D. Tlsty and A. J. Engler, Metastatic State of Cancer Cells May Be Indicated by Adhesion Strength, *Biophys. J.*, 2017, **112**(4), 736–745, DOI: 10.1016/j.bpj.2016.12.038.
16 N. Paddillaya, A. Mishra, P. Kondaiah, P. Pullarkat, G. I. Menon and N. Gundiah, Biophysics of cell-substrate interactions under shear, *Front. Cell Dev. Biol.*, 2019, **7**, 251.
17 R. Maan, G. Rani, G. I. Menon and P. A. Pullarkat, Modeling cell-substrate de-adhesion dynamics under fluid shear, *Phys. Biol.*, 2018, **15**(4), 046006, DOI: 10.1088/1478-3975/aabc66.
18 A. Fuhrmann, J. Li, S. Chien and A. J. Engler, Cation type specific cell remodeling regulates attachment strength, *PLoS One*, 2014, **9**(7), e102424, DOI: 10.1371/journal.pone.0102424.
19 P. Beri, A. Popravko, B. Yeoman, A. Kumar, K. Chen, E. Hodzic, A. Chiang, A. Banisadr, J. K. Placone, H. Carter, S. I. Fraley, P. Katira and A. J. Engler, Cell adhesiveness serves as a biophysical marker for metastatic potential, *Cancer Res.*, 2020, **80**(4), 901–911, DOI: 10.1158/0008-5472.CAN-19-1794.
20 C. M. Kraning-Rush, J. P. Califano and C. A. Reinhart-King, Cellular traction stresses increase with increasing metastatic potential, *PLoS One*, 2012, **7**(2), e32572, DOI: 10.1371/journal.pone.0032572.
21 A. H. Kulkarni, P. Ghosh, A. Seetharaman, P. Kondaiah and N. Gundiah, Traction cytometry: Regularization in the Fourier approach and comparisons with finite element method, *Soft Matter*, 2018, **14**(23), 4687–4695, DOI: 10.1039/c7sm02214j.
22 P. Ranganathan, A. Agrawal, R. Bhushan, A. K. Chavalmane, R. K. R. Kalathur and T. Takahashi, Expression profiling of genes regulated by TGF-beta: Differential regulation in normal and tumour cells, *BMC Genomics*, 2007, **8**, 98, DOI: 10.1186/1471-2164-8-98/FIGURES/8.
23 P. A. Pullarkat, R. Vishavkarma, N. Gundiah and N. Chahare, *A microscope mountable fluid shear device*, IN201641029893A, 2016.
24 G. I. Bell, Models for the specific adhesion of cells to cells, *Science*, 1978, **200**(4342), 618–627, DOI: 10.1126/science.347575.
25 J. R. Tse and A. J. Engler, Preparation of hydrogel substrates with tunable mechanical properties, *Curr. Protoc. Cell Biol.*, 2010, **47**, 10–16, DOI: 10.1002/0471143030.cb1016s47.
26 A. Fuhrmann and A. J. Engler, The Cytoskeleton Regulates Cell Attachment Strength, *Biophys. J.*, 2015, **109**(1), 57–65, DOI: 10.1016/j.bpj.2015.06.003.
27 D. Boettiger, L. Lynch, S. Blystone and F. Huber, Distinct ligand-binding modes for integrin αvβ 3-mediated adhesion to fibronectin versus vitronectin, *J. Biol. Chem.*, 2001, **276**(34), 31684–31690, DOI: 10.1074/jbc.M103997200.
28 A. S. Goldstein and P. A. DiMilla, Effect of adsorbed fibronectin concentration on cell adhesion and deformation under shear on hydrophobic surfaces, *J. Biomed. Mater. Res.*, 2002, **59**(4), 665–675, DOI: 10.1002/jbm.1276.
29 D. Wirtz, K. Konstantopoulos and P. C. Searson, The physics of cancer: The role of physical interactions and mechanical forces in metastasis, *Nat. Rev. Cancer*, 2011, **11**(7), 512–522, DOI: 10.1038/nrc3080.
30 A. Spencer and A. B. Baker, High throughput label free measurement of cancer cell adhesion kinetics under hemodynamic flow, *Sci. Rep.*, 2016, **6**, 19854, DOI: 10.1038/srep19854.
31 C. Spangenberg, E. U. Lausch, T. M. Trost, D. Prawitt, A. May, R. Keppler, S. A. Fees, D. Reutzel, C. Bell, S. Schmitt, I. B. Schiffer, A. Weber, W. Brenner, M. Hermes, U. Sahin, O. Türeci, H. Koelbl, J. G. Hengstler and B. U. Zabel, ERBB2-mediated transcriptional up-regulation of the α5β1 integrin fibronectin receptor promotes tumor cell survival under adverse conditions, *Cancer Res.*, 2006, **66**(7), 3715–3725, DOI: 10.1158/0008-5472.CAN-05-2823.
32 J. X. Zou, Y. Liu, E. B. Pasquale and E. Ruoslahti, Activated Src oncogene phosphorylates R-Ras and suppresses integrin activity, *J. Biol. Chem.*, 2002, **277**(3), 1824–1827, DOI: 10.1074/jbc.M103133200.
33 E. M. Balzer, R. A. Whipple, E. H. Cho, M. A. Matrone and S. S. Martin, Antimitotic chemotherapeutics promote adhesive responses in detached and circulating tumor cells, *Breast Cancer Res. Treat.*, 2010, **121**(1), 65–78, DOI: 10.1007/s10549-009-0457-3.
34 J. Haier and G. L. Nicolson, Tumor cell adhesion of human colon carcinoma cells with different metastatic properties to extracellular matrix under dynamic conditions of laminar flow, *J. Cancer Res. Clin. Oncol.*, 2000, **126**(1), 699–706, DOI: 10.1007/s004320000161.
35 A. Fuhrmann and A. J. Engler, Acute shear stress direction dictates adherent cell remodeling and verifies shear profile of spinning disk assays, *Phys. Biol.*, 2015, **12**(1), 016011, DOI: 10.1088/1478-3975/12/1/016011.
36 S. P. Palecek, J. C. Loftust, M. H. Ginsberg, D. A. Lauffenburger and A. F. Horwitz, Integrin-ligand binding properties govern cell migration speed through cell-substratum adhesiveness, *Nature*, 1997, **385**(6616), 537–540, DOI: 10.1038/385537a0.
37 C. S. Chen, J. L. Alonso, E. Ostuni, G. M. Whitesides and D. E. Ingber, Cell shape provides global control of focal adhesion assembly, *Biochem. Biophys. Res. Commun.*, 2003, **307**(2), 355–361, DOI: 10.1016/S0006-291X(03)01165-3.
38 R. McBeath, D. M. Pirone, C. M. Nelson, K. Bhadriraju and C. S. Chen, Cell shape, cytoskeletal tension, and RhoA regulate stem cell lineage commitment, *Dev. Cell*, 2004, **6**(4), 483–495, DOI: 10.1016/S1534-5807(04)00075-9.
39 J. P. Butler, I. M. Toli-Nørrelykke, B. Fabry and J. J. Fredberg, Traction fields, moments, and strain energy that cells exert on their surroundings, *Am. J. Physiol.: Cell Physiol.*, 2002, **282**(3), C595–C605, DOI: 10.1152/AJPCELL.00270.2001.
40 K. Ghosh, C. K. Thodeti, A. C. Dudley, A. Mammoto, M. Klagsbrun and D. E. Ingber, Tumor-derived endothelial

cells exhibit aberrant Rho-mediated mechanosensing and abnormal angiogenesis in vitro, *Proc. Natl. Acad. Sci. U. S. A.*, 2008, **105**(32), 11305–11310, DOI: **10.1073/pnas.0800835105**.

41 S. Munevar, Y. L. Wang and M. Dembo, Traction force microscopy of migrating normal and H-ras transformed 3T3 fibroblasts, *Biophys. J.*, 2001, **80**(4), 1744–1757, DOI: **10.1016/S0006-3495(01)76145-0**.

42 H. H. Lin, H. K. Lin, I. H. Lin, Y. W. Chiou, H. W. Chen, C. Y. Liu, H. I. Harn, W. T. Chiu, Y. K. Wang, M. R. Shen and M. J. Tang, Mechanical phenotype of cancer cells: Cell softening and loss of stiffness sensing, *Oncotarget*, 2015, **6**(25), 20946–20958, DOI: **10.18632/oncotarget.4173**.

43 T. M. Koch, S. Münster, N. Bonakdar, J. P. Butler and B. Fabry, 3D traction forces in cancer cell invasion, *PLoS One*, 2012, **7**(3), e33476, DOI: **10.1371/journal.pone.0033476**.

44 S. Sen and S. Kumar, Cell-matrix de-adhesion dynamics reflect contractile mechanics, *Cell. Mol. Bioeng.*, 2009, **2**(2), 218–230, DOI: **10.1007/S12195-009-0057-7**.

45 V. Peschetola, V. M. Laurent, A. Duperray, R. Michel, D. Ambrosi, L. Preziosi and C. Verdier, Time-dependent traction force microscopy for cancer cells as a measure of invasiveness, *Cytoskeleton*, 2013, **70**(4), 201–214, DOI: **10.1002/cm.21100**.

46 V. Vasioukhin, Adherens junctions and cancer, *Subcell. Biochem.*, 2012, **60**, 379–414, DOI: **10.1007/978-94-007-4186-7_16**.

47 J. P. Their, Epithelial-mesenchymal transitions in tumor progression, *Nat. Rev. Cancer*, 2002, **74**, 1–15, DOI: **10.1038/nrc822**.

48 D. E. Discher, P. Janmey and Y. L. Wang, Tissue cells feel and respond to the stiffness of their substrate, *Science*, 2005, **310**(5751), 1139–1143, DOI: **10.1126/science.1116995**.

49 D. R. Welch, Tumor heterogeneity - A ''contemporary concept'' founded on historical insights and predictions, *Cancer Res.*, 2016, **76**(1), 4–6, DOI: **10.1158/0008-5472.CAN-15-3024**.

50 O. Chaudhuri, L. Gu, M. Darnell, D. Klumpers, S. A. Bencherif, J. C. Weaver, N. Huebsch and D. J. Mooney, Substrate stress relaxation regulates cell spreading, *Nat. Commun.*, 2015, **6**, 6364, DOI: **10.1038/ncomms7365**.

51 V. Vogel and M. Sheetz, Local force and geometry sensing regulate cell functions, *Nat. Rev. Mol. Cell Biol.*, 2006, **7**(4), 265–275, DOI: **10.1038/nrm1890**.

52 P. Pakshir, M. Alizadehgiashi, B. Wong, N. M. Coelho, X. Chen, Z. Gong, V. B. Shenoy, C. A. McCulloch and B. Hinz, Dynamic fibroblast contractions attract remote macrophages in fibrillar collagen matrix, *Nat. Commun.*, 2019, **10**(1), 1850, DOI: **10.1038/s41467-019-09709-6**.

53 S. Van Helvert, C. Storm and P. Friedl, Mechanoreciprocity in cell migration, *Nat. Cell Biol.*, 2018, **20**(1), 8–20, DOI: **10.1038/s41556-017-0012-0**.

54 J. Fares, M. Y. Fares, H. H. Khachfe, H. A. Salhab and Y. Fares, Molecular principles of metastasis: a hallmark of cancer revisited, *Signal Transduction Targeted Ther.*, 2020, **5**(1), 28, DOI: **10.1038/s41392-020-0134-x**2020 51.

55 S. L. Gupton and C. M. Waterman-Storer, Spatiotemporal feedback between actomyosin and focal-adhesion systems optimizes rapid cell migration, *Cell*, 2006, **125**(7), 1361–1374, DOI: **10.1016/j.cell.2006.05.029**.

